



UNIVERSITY OF LEEDS

This is a repository copy of *On the Origin of Anomalous Eutectic Growth from Undercooled Melts: Why Re-melting is not a Plausible Explanation*.

White Rose Research Online URL for this paper:  
<http://eprints.whiterose.ac.uk/125425/>

Version: Accepted Version

---

**Article:**

Mullis, AM and Clopet, CR (2018) On the Origin of Anomalous Eutectic Growth from Undercooled Melts: Why Re-melting is not a Plausible Explanation. *Acta Materialia*, 145. pp. 186-195. ISSN 1359-6454

<https://doi.org/10.1016/j.actamat.2017.12.016>

---

© 2017, Acta Materialia Inc. Published by Elsevier Ltd. Licensed under the Creative Commons Attribution-NonCommercial-NoDerivatives 4.0 International  
<http://creativecommons.org/licenses/by-nc-nd/4.0/>

**Reuse**

This article is distributed under the terms of the Creative Commons Attribution-NonCommercial-NoDeriv (CC BY-NC-ND) licence. This licence only allows you to download this work and share it with others as long as you credit the authors, but you can't change the article in any way or use it commercially. More information and the full terms of the licence here: <https://creativecommons.org/licenses/>

**Takedown**

If you consider content in White Rose Research Online to be in breach of UK law, please notify us by emailing [eprints@whiterose.ac.uk](mailto:eprints@whiterose.ac.uk) including the URL of the record and the reason for the withdrawal request.



[eprints@whiterose.ac.uk](mailto:eprints@whiterose.ac.uk)  
<https://eprints.whiterose.ac.uk/>

# On the Origin of Anomalous Eutectic Growth from Undercooled Melts: Why Re-melting is not a Plausible Explanation

*Andrew M Mullis & Caroline R Clopet*

School of Chemical & Process Engineering, University of Leeds, Leeds LS2 9JT, UK.

**Keywords:** Rapid solidification; Anomalous eutectic; Image analysis.

## *Abstract*

Ag-Cu melt at the equilibrium eutectic composition has been undercooled using a melt fluxing technique. The resulting samples have been sectioned through the nucleation point and the spatial distribution of anomalous eutectic has been quantified. This is shown to be highly inhomogeneous, with the volume of anomalous material decreasing approximately linearly with distance from the nucleation site. In samples at low undercooling the volume fraction of anomalous eutectic near the nucleation site is around an order of magnitude greater than the calculated recalescence solid fraction. As such, any model for the origin of the anomalous eutectic invoking *partial* remelting of this initial solid is shown to be infeasible. An alternative model, based on a kinetic shift of the eutectic point during rapid solidification is proposed.

## **1. Introduction**

It is well documented that many binary eutectic alloys, when solidified from their undercooled parent melt, will solidify to a morphology known as the anomalous eutectic. Systems demonstrated to show this behaviour include Ag-Cu [1, 2, 3, 4, 5], Co-Al [6], Co-Mo [7], Co-Sb [8], Co-Sn [9], Ni-Si [6, 8] and Ni-Sn [10, 11, 12]. The anomalous eutectic morphology is typically much coarser and more globular than the equilibrium eutectic morphology (lamellar or rod like, depending upon system), with which it can coexist. Salient features of anomalous eutectic formation which appear to be established beyond doubt are that the volume fraction of the anomalous morphology tends to increase with increasing undercooling [2, 3, 4] and that the spatial distribution of the anomalous morphology is inhomogeneous within the undercooled sample. Indeed, many samples have been shown to contain a greater abundance of anomalous material near the nucleation point [4, 5], with zones of anomalous eutectic radiating outwards from the nucleation point. This spatial inhomogeneity of the anomalous eutectic has however not been properly quantified.

The origin of the anomalous eutectic has been the subject of considerable interest since the morphology was first identified in the 1960's. Models proposed to account for its formation include those based around the effect of impurity ions [1], multiple nucleation ahead of the eutectic front [10], direct growth of the anomalous morphology, either via coupled [13] or uncoupled (non-cooperative) [3, 7, 11, 14] growth and remelting/fragmentation mechanisms. Remelting and

fragmentation has been proposed to occur within the lamellar eutectic [4, 8, 9, 15], single phase dendrites [16] and eutectic cells or dendrites [12, 17], with the remelting of single phase or eutectic dendrites currently being the most popular explanations within the literature. Indeed, a number of authors have proposed a dual mechanism to account for differences in anomalous eutectic morphologies observed at high and low undercooling, with remelting of eutectic dendrites at low undercooling and remelting of single phase dendrites at high undercooling (typically  $\geq 200$  K) [12, 18]. Wei *et al.* [19] have extended this idea, arguing that the type of remelting also depends upon the alloy system being studied, with a complex relationship between the alloy phase diagram and the type of remelting being invoked. However, as pointed out by [20], there are few systems in which eutectic growth is reported at undercoolings  $\geq 200$  K, these being limited to systems in which at least one phase is an intermetallic compound. Recently Lai *et al.* [21] have demonstrated that in the Ni-Si system anomalous eutectic formation is accompanied by a double recalescence event, a phenomenon also observed in Ag-Cu [5].

It appears to us though that there is a fundamental problem with all remelting models for anomalous eutectic formation at low undercooling. Remelting is, by definition, restricted to the solid formed during the recalescence phase of solidification of the undercooled melt, with the recalescence solid fraction being determined by the undercooling at nucleation. Yet we are aware of instances in which eutectic alloys solidified at low undercoolings display anomalous eutectic with volume fractions which are far in excess of any reasonable estimate of the recalescence solid fraction. The objective of this paper is therefore to develop and apply a methodology for the quantification of the anomalous eutectic fraction within a eutectic microstructure and to hence map the spatially inhomogeneous distribution of anomalous material within eutectic samples as a function of both bulk undercooling and distance from the nucleation point. Measurement and spatial mapping of the lamellar spacing (in the lamellar eutectic fraction) is also employed as a means of evaluating the variation of undercooling within the sample during solidification.

We illustrate this methodology with reference to the Ag-Cu system which, as discussed below, provides appropriate contrast when imaged in backscatter mode in the SEM for correct application of the analysis methodology. The Ag-Cu phase diagram, including metastable extensions [22] and coupled zone adopted from [23], is shown in Figure 1. At the eutectic composition the  $T_0$ -line is some 75 K below the eutectic temperature and extensive formation of single phase Ag-rich dendrites is observed for undercoolings in excess of 70-76 K [2, 5].

## 2. Experimental Methods

Ag-Cu alloy of eutectic composition was produced by melting together high purity (Alfa Aesar, 99.9999% metals basis) Ag and Cu shot sealed into a silica tube under a protective argon atmosphere. The resulting alloy was allowed to cool naturally before being remelted, with the melting  $\rightarrow$  mixing  $\rightarrow$  solidification cycle being repeated 4 times. At the end of the final mixing cycle the tube was quenched into water and the ingot broken out of the tube. Prior to rapid solidification

processing the alloy was sectioned and a sample prepared for metallographic examination. SEM and EDX was used to check that the resulting alloy comprised a homogeneous eutectic microstructure of the correct composition.

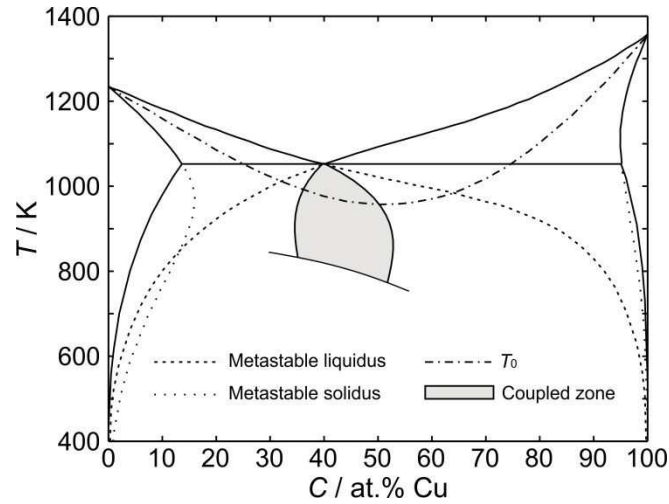


**Figure 1.** Phase diagram for the Ag-Cu system including metastable extensions and  $T_0$ -line (after [22]) and coupled zone as determined by [23].

Undercooling of the melt was performed using a melt fluxing technique, with approximately 0.8 g of the alloy being used for each experiment. The alloy is contained within a fused silica crucible which is first etched with a 7 vol.% solution of HF acid to remove any microcracks from the inner surface. The crucible is packed with a layer of finely ground flux before the sample is placed in the crucible, with further flux packed on top of the sample. A 50 wt.% mixture of dehydrated  $B_2O_3$  and soda-lime glass was used as the fluxing agent as this has sufficient viscosity to support the sample when superheated above the eutectic temperature, remains fluid when the sample is undercooled and is inert with respect to the molten eutectic.

Undercooling experiments were performed under a high purity inert atmosphere within a stainless steel vacuum chamber evacuated to  $10^{-4}$  Pa and backfilled with 50 kPa of high purity, oxygen free  $N_2$  gas. The crucible containing the sample and flux sits inside a graphite susceptor which is contained within an alumina heat shield. Heating of the susceptor is by means of an induction coil, connected to a 450 kHz RF power supply. The susceptor is large relative to the crucible (susceptor, 119 mm high by 33 mm id, crucible 20 mm high by 7 mm id), wherein the sample and crucible experience uniform blackbody heating by the susceptor, minimising temperature gradients experienced by the sample. In addition, the high temperature graphite also serves to reduce any stray oxygen or water vapour within the system and shield the sample from direct RF heating and stirring by the induction field. Temperature determination was by means of an R-type thermocouple placed in the base of the crucible, which had been thinned so as to ensure good thermal contact. Further details of the experimental setup are given in [24].

During the undercooling experiments the melt was heated to 1350 K, with the superheat being

held at this level for 11 minutes, after which time the system was allowed to cool at an average cooling rate of  $10 \text{ K min}^{-1}$ . Sample nucleation was allowed to occur spontaneously. For the higher undercoolings reported it was necessary to repeat the melting  $\rightarrow$  solidification cycle a number of times until the desired level of undercooling was attained. An increase in undercooling with repeated cycling is not uncommon during flux undercooling experiments [25].

Once cool the sample was removed from the vacuum system and broken out of the flux. The nucleation site was identified using optical microscopy and the sample sectioned through the nucleation point, with the resulting section being mounted and polished for metallographic examination. Microstructural examination was by means of a Carl Zeiss Evo® MA 15 SEM operating in back-scatter detection mode at an accelerating voltage of 20 kV. In order to construct maps of the distribution of anomalous eutectic within the sectioned droplet typically 20-25 images were obtained from different regions on the polished surface of the sample. A typical sampling pattern, in this case for a droplet undercooled by 19 K, is shown in Figure 2. The perimeter of the droplet in the figure has been digitally traced from a low magnification micrograph and accurately reflects the non-spherical shape of the sectioned sample.

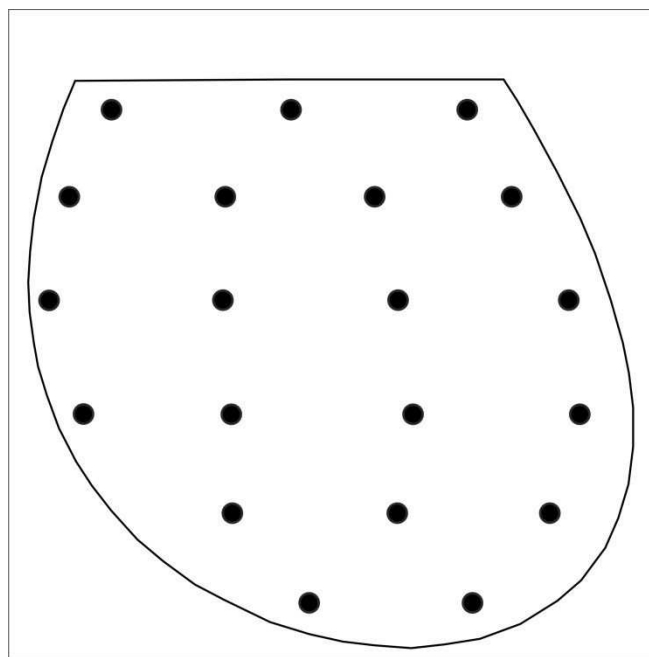


**Figure 2.** Sampling pattern illustrated for the sample undercooled by 19 K.

A typical back-scatter micrograph from the sample undercooled by 19 K is shown in Figure 3a and comprises a mixture of fine lamellar eutectic interspersed with a much coarser anomalous eutectic. Within the lamellar region the average lamellar spacing was measured in four separate regions, with each measurement encompassing at least 10 lamellae. In order to automatically detect the anomalous eutectic we make use of the fact that the anomalous material is much coarser than the standard lamellar eutectic. Indeed, with an accelerating voltage of 20 kV the individual lamellae are barely resolved due to the large interaction volume of the high energy backscatter electrons.

Normally, resolution would be increased by decreasing the accelerating voltage (confirmed by imaging at 5 kV), but here we utilise this poor resolution. By applying a Gaussian blur filter to the image, resolution of the individual Ag- and Cu-rich lamellae is lost and the lamellar eutectic is rendered a uniform grey (Figure 3b). We now use the grey level in the resulting image to identify the Cu- and Ag-rich regions in the coarse anomalous eutectic from the (now unresolved) lamellar eutectic as shown in (Figure 3c). By repeating this process at each location shown in Figure 2, a map of the spatial distribution of anomalous eutectic can be constructed.

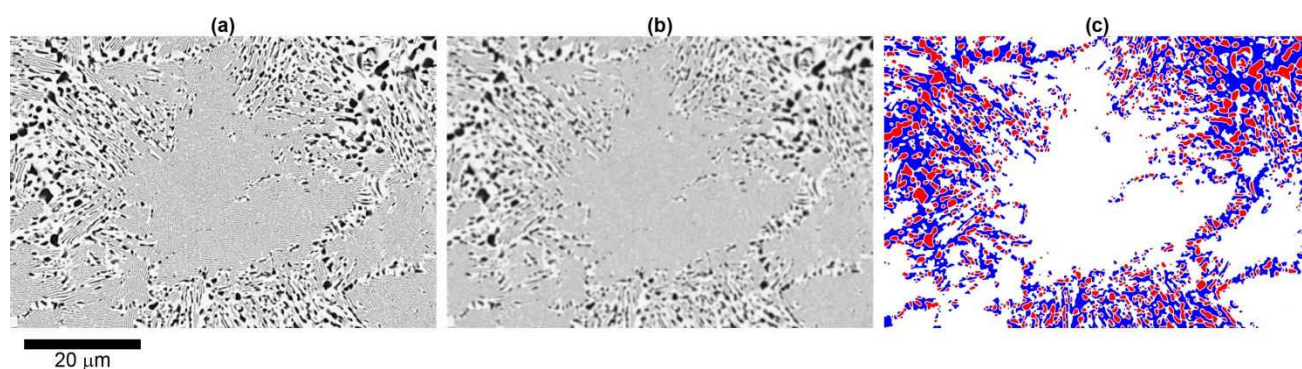


**Figure 3.** Illustration of the image analysis technique used to quantify the volume fraction of anomalous material: (a) SEM backscatter micrograph, (b) application of Gaussian blur, lamellar eutectic is rendered uniform mid-grey, (c) grey scale threshold detection identified anomalous (Cu-rich red and Ag-rich blue) eutectic from lamellar eutectic (white).

### 3. Results

Figure 4 gives maps for the spatial distribution of anomalous eutectic within droplets undercooled by (a)  $\Delta T = 10$  K, (b)  $\Delta T = 19$  K, (c)  $\Delta T = 27$  K and (d)  $\Delta T = 51$  K with, in each case, the map giving the volume fraction,  $f_a$ , of anomalous material. In each case the droplet was sectioned close to the nucleation point and, as far as could be determined, parallel to the growth direction. Two features in particular are worthy of note with respect to these maps. The first is the extreme inhomogeneity in the spatial distribution of the anomalous material and the second is the high volume fraction of anomalous eutectic measured near the nucleation point. Each is considered in more detail below.

A number of authors [4, 26] have commented previously on the fact that the anomalous eutectic is most pronounced near the nucleation point and that its prevalence tends to decrease the further one moves away from the nucleation point. However, as far as we are aware, the extreme nature of this variation with distance from the nucleation point has not previously been quantified. Further details on the nature of the variation are shown in Figure 5 which plots the fraction of anomalous eutectic as a function of the scaled distance from the nucleation point for (a)  $\Delta T = 10$  K, and (b)  $\Delta T = 27$  K. In both cases the distance is scaled against the maximum diameter of the droplet and an approximate, but clear, linear trend may be observed. Such variation within Ag-Cu samples has previously been attributed [4] to the combination of the high thermal diffusivity of the melt and the slow growth rate of the eutectic, resulting in a large thermal boundary layer ahead of the growth front. This will result

in warming of the sample ahead of the growth front with a consequent reduction in undercooling as solidification proceeds, leading to non-steady-state growth.

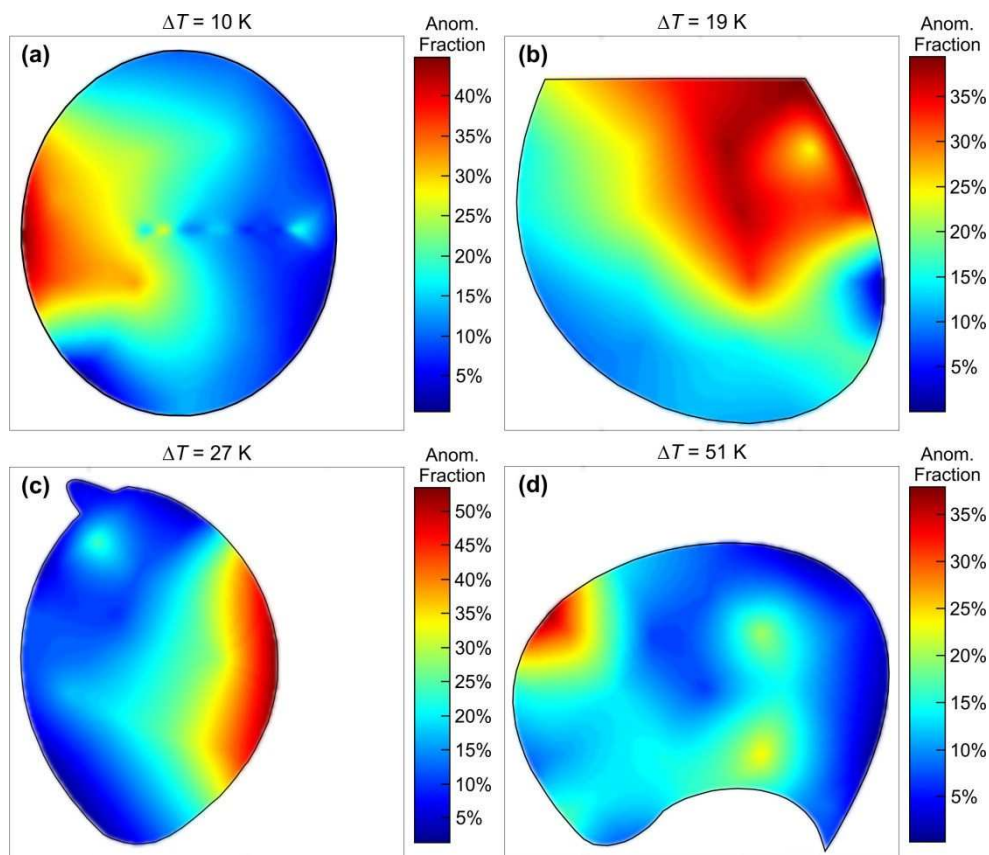


**Figure 4.** Spatial maps of anomalous eutectic fraction for samples undercooled by (a) 10 K, (b) 19 K, (c) 27 K and (d) 51 K.

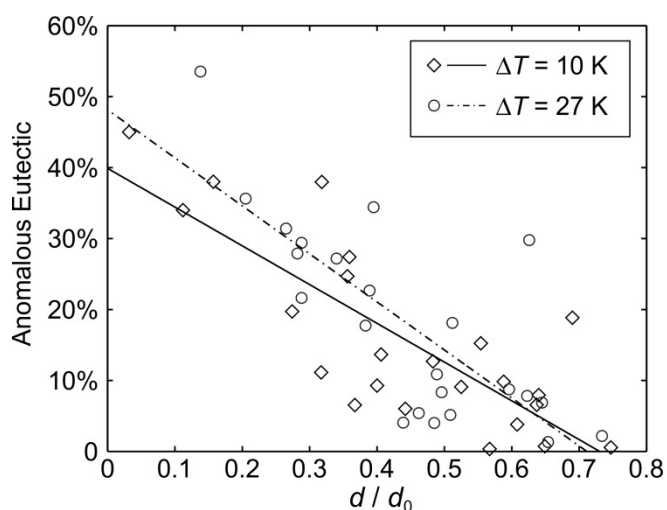


**Figure 5.** Plot of anomalous eutectic fraction as a function of distance from the nucleation point scaled by the maximum apparent droplet diameter,  $d_0$ , for samples undercooled by 10 and 27 K.

Measurement of the lamellar spacing,  $\lambda$ , within the lamella eutectic fraction, of these samples can be used to understand the variation of undercooling within the droplet as recalescence proceeds. This is contoured, as a function of position within the sample, in Figure 6 a&b where, for the sake of brevity, we show only the results for  $\Delta T = 10$  K and  $\Delta T = 51$  K, these being the lowest and highest undercoolings studied respectively. The lamellar spacing at the extremum,  $\lambda_e$ , may be related to the corresponding extremum undercooling at the interface,  $\Delta T_i$ , by the Jackson & Hunt relationship [27]

$$\lambda_e \Delta T_i = K \quad (1)$$

where the constant  $K$  has been estimated experimentally by Walder & Ryder [2] as  $4.3 \times 10^{-7}$  K m. Using Equ. (1) to convert the measured values of  $\lambda$  to a corresponding undercooling we obtain the contour maps shown in Figure 6 c&d, wherein we note the good spatial correlation with the equivalent maps for anomalous eutectic fraction (Figure 4 a&d). The undercooling at the eutectic front,  $\Delta T_e$ , will be one component of the bulk undercooling,  $\Delta T$ , according to

$$\Delta T = \Delta T_i + \Delta T_c + \Delta T_r \quad (2)$$

where  $\Delta T_c$  and  $\Delta T_r$  are the solutal and curvature components of the undercooling respectively. As it is predicted [27] that  $\Delta T_i$  will increase monotonically with increasing  $\Delta T$ , the contour maps shown in Figure 6 c&d provide strong evidence that the bulk undercooling is indeed decreasing with distance from the nucleation point. Moreover, the correlation between the volume fraction of anomalous eutectic observed and the calculated interfacial undercooling, suggests that the abundance of the anomalous eutectic is decreasing with distance from the nucleation point because the bulk undercooling is decreasing as recalescence proceeds. The correlation is strong but not exact and this we believe is due to the difficulty in making accurate measurements of eutectic lamellar spacing. Specifically, the true spacing will be measured only if the eutectic is sectioned perpendicular to the lamellar orientation, with the spacing always being overestimated, and hence the interfacial undercooling underestimated, if the section is not perpendicular.

We now return to the maximum abundance of anomalous eutectic. The maximum value of  $f_a$  in the samples shown in Figure 4 is 53.5% at  $\Delta T = 27$  K, although due to the inhomogeneity in the distribution of anomalous material each map should be considered as giving the lower bounds on the maximum anomalous fraction. In particular, small variations in sectioning correctly through the nucleation point and the distance of the first sampling point from the nucleation point could significantly affect the observed maximum for a given sample. For this reason it is not clear whether there is any significance to the fact that the sample with the highest observed  $f_a$  (53.5% anomalous eutectic) is not most deeply undercooled of the samples, the observed maximum anomalous fraction in the sample at  $\Delta T = 51$  K being  $f_a = 44.4\%$ .

The composition of the Ag- and Cu-rich phases within the anomalous eutectic has been checked using EDX with a typical EDX map, in this case for a sample undercooled by  $\Delta T = 51$  K, being given in Figure 7. Various spot measurements have been made in both the Ag- and Cu-rich regions with the mean composition found to be 4.7 at.% Ag in the Cu-rich phase and 13.9 at.% Cu in the Ag-

rich phase, with similar values being found across all samples. These values are very close to those expected at equilibrium and with reference to the metastable phase diagram (Figure 1) are consistent with growth of the anomalous eutectic at very low undercooling.

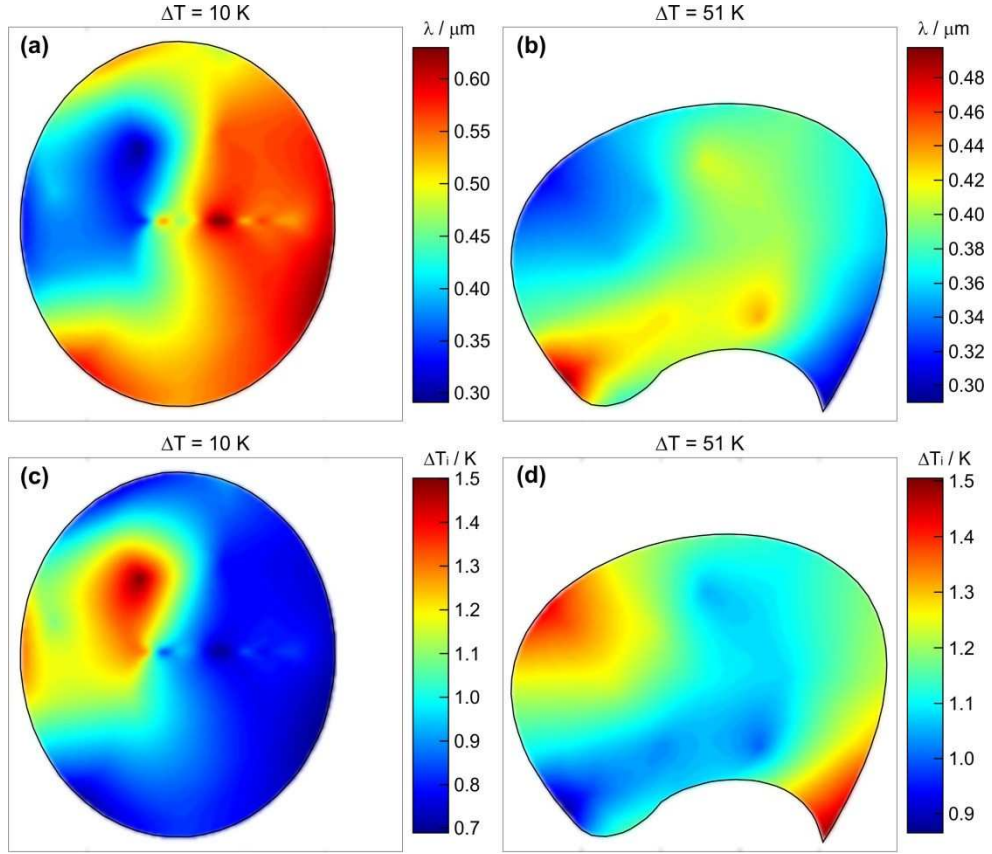


**Figure 6.** (a & b) Mean spacing,  $\lambda$ , as measured in the lamellar eutectic fraction of samples undercooled by 10 and 51 K respectively and (c & d) corresponding interface undercooled for extremum growth [27].

In terms of models for the origin of the anomalous eutectic the high values of  $f_a$  measured near the droplet nucleation points in this study have profound implications. As discussed above, virtually all models for the formation of the anomalous eutectic involve *partial* remelting of material formed during the initial recalescence stage of solidification. For instance Wei *et al.* [19] propose a model in which *partial* remelting of the primary solid, either in the form of eutectic or single-phase dendrites, during the solidification of undercooled eutectic melts gives rise to the anomalous eutectic. They argue, at least in relation to solid-solution phases such Ag-Cu that ‘The primary solid, whether it is in the form of a eutectic or single-phase structure, is supersaturated with solute and will partially remelt during temperature recalescence’. However, the volume of anomalous material observed here is simply far too high for this, or indeed any remelting mechanism, to be at all plausible. The fraction solid formed during recalescence of a melt undercooled to a temperature  $T_N$  is given by:

$$f_S = \frac{\int_{T_N}^{T_E} c_p(T) dT}{H_f} \approx \frac{c_p(T_E)(T_E - T_N)}{H_f} = \frac{c_p(T_E)\Delta T}{H_f} \quad (3)$$

Where  $T_E$  is the eutectic temperature,  $c_p(T)$  is the heat capacity of the liquid and  $H_f = H_S - H_L$  is the heat of fusion. Both can be obtained from the Gibbs free energy,  $G$ , for the system via:

$$c_p(T) = -T \frac{\partial^2 G_L}{\partial T^2} \quad \text{and} \quad H_{L,S} = -T^2 \left. \frac{\partial(G_{L,S}/T)}{\partial T} \right|_{T_E} \quad (4)$$

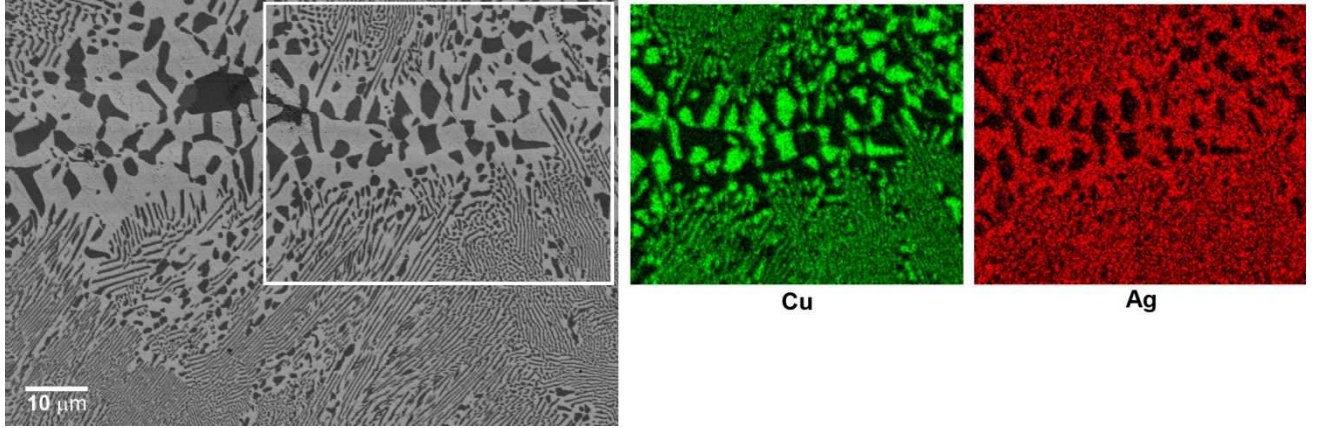


**Figure 7.** EDX map (Ag and Cu) of a sample undercooled by 51 K prior to nucleation.

The Ag-Cu system has been subject to rigorous thermodynamic assessment, meaning  $G$  is known very accurately over the whole composition range and for a wide range of temperatures [28]. To a very good approximation Equations (4) give  $c_p = (30.23779 - 0.00885\Delta T) \text{ J mol}^{-1} \text{ K}^{-1}$ , and  $H_f = 8808.7 \text{ J mol}^{-1}$ , wherein we calculate  $f_s$  as ranging from 3.4% at  $\Delta T = 10 \text{ K}$  to 17.4% at  $\Delta T = 51 \text{ K}$ . In all cases the solid fraction formed during primary solidification is very significantly less than the observed volume fraction of anomalous material, whereby *partial* remelting cannot account for the high fractions of anomalous material observed.

To reinforce this point, Figure 8a gives a map of the anomalous eutectic fraction observed in a droplet undercooled by  $\Delta T = 40 \text{ K}$ . For this sample a nucleation point could not be identified on the surface of the droplet but on sectioning very high volumes of anomalous material were observed. The maximum in  $f_a$  occurs in the middle of the droplet, not near the surface, possibly indicating nucleation in the interior of the droplet. Notwithstanding this, the observed maximum value of  $f_a$  is 87.4%. The original micrograph taken at the location of the maximum is shown in Figure 8b, wherein the relatively small proportion of ‘normal’ lamellar eutectic, mostly confined to the centre of the micrograph, is apparent. The calculated primary solidification fraction,  $f_s$ , at  $\Delta T = 40 \text{ K}$  is 13.7%. In light of these findings an alternative model for anomalous eutectic formation, not invoking partial remelting of the primary solid, will be considered in the next section.

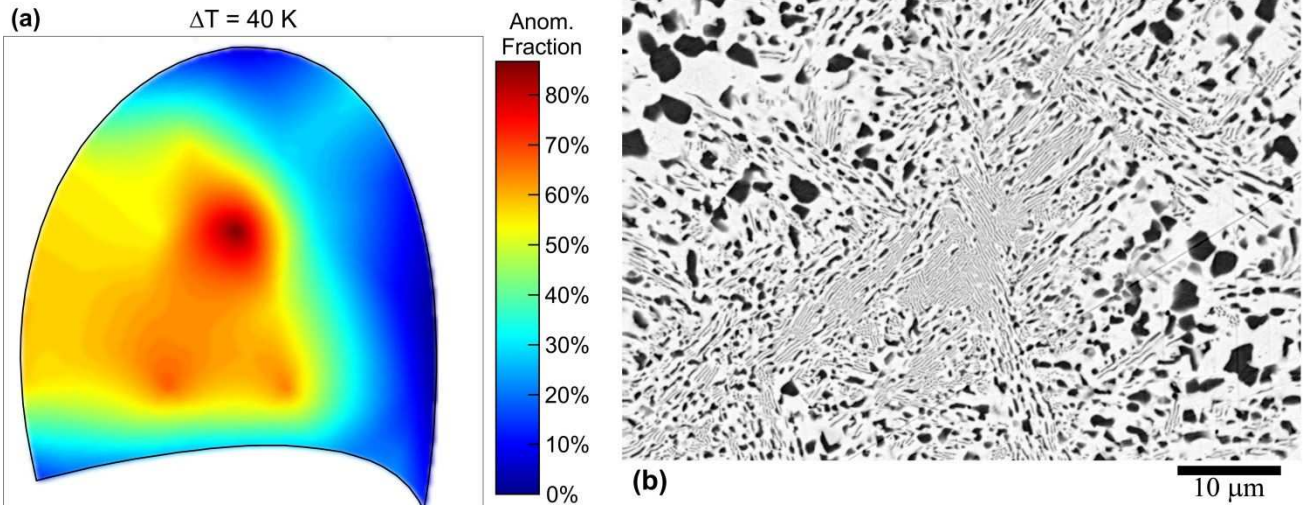


**Figure 8.** (a) Spatial map of anomalous eutectic fraction for a samples undercooled by 40 K. Surface nucleation point could not be identified, interior nucleation looks likely and (b) micrograph showing 87% volume fraction anomalous eutectic.

#### 4. Discussion and Analysis

Given that partial remelting of the primary solidification phase(s), be that of single-phase dendrites, eutectic dendrites, or lamellar eutectic, is not a plausible explanation for the formation of the anomalous eutectic, the volume fraction of solid formed during recalescence being too low, we now explore other possibilities. If the anomalous eutectic is not the result of remelting, the likelihood would seem that it is formed as a primary solidification phase either during, or shortly after, recalescence. Such models have previously been proposed for both de-coupled [3, 7, 10] and coupled [13] growth of the two phases. Of course, any such model needs to explain why the anomalous eutectic is favoured as a primary solidification morphology over the normal lamellar structure.

Recently, Wang and co-workers [29] have presented a model for the rapid solidification of eutectic melts which includes the kinetics of the eutectic triple junction, thereby allowing them to calculate the effect of growth velocity on the location of the eutectic point. This has been extended by Kuang *et al.* [30] to model the growth of eutectic dendrites within the framework of a non-equilibrium solidification model, including a finite velocity,  $V_D$ , for solute diffusion in the bulk. For growth at velocity  $V$ , the composition of the eutectic point,  $C_E$ , on the assumption of negligible interface attachment kinetics for the  $\alpha$  (Ag-rich) and  $\beta$  (Cu-rich) phases is given by:

$$C_E = \frac{m_{L\beta} - m_{L\alpha}^e C_E^e - m_{L\beta}^e (1 - C_E^e)}{m_{L\beta} - m_{L\alpha}} \quad (5)$$

where  $C_E^e$  is the equilibrium eutectic concentration,  $m_{L\alpha}^e$ ,  $m_{L\beta}^e$ ,  $m_{L\alpha}$  and  $m_{L\beta}$  are the equilibrium and velocity dependent liquidus slopes for the  $\alpha$  and  $\beta$  phases respectively, with:

$$m_{Lj} = \frac{m_{Lj}^e}{1 - k_j^e} \left\{ 1 - k_j + \ln \left( \frac{k_j}{k_j^e} \right) + (1 - k_j)^2 \frac{V}{V_D} \right\} \quad j = \alpha, \beta \quad (6)$$

In [30] the authors omitted the final term within the braces, although for completeness a model incorporating hyperbolic diffusion should include this term [31], which is done here.  $k_\alpha^e$ ,  $k_\beta^e$ ,  $k_\alpha$  and  $k_\beta$  are the equilibrium and velocity dependent partition coefficients, which for a characteristic velocity for diffusion at the solid-liquid interface,  $V_{DI}$ , (as distinct for  $V_D$ , which is in the bulk liquid) are:

$$k_j = \frac{V/V_{DI} + k_j^e \psi}{V/V_{DI} + \psi} \quad j = \alpha, \beta \quad (7)$$

with  $\psi = 1 - V^2/V_D^2$ . As above, [30] does not distinguish between  $V_D$  and  $V_{DI}$ , although as pointed out by [32] a full treatment of the effect should do so. Consequently, this has been incorporated here with  $V_{DI}$  being taken as  $0.8 V_D$ , in line with values used in [32].

Evaluating Equation (5) for the Ag-Cu system with  $m_{L\alpha}^e = -4.60$  K/at.%,  $m_{L\beta}^e = 5.02$  K/at.%,  $k_\alpha^e = 0.342$ ,  $k_\beta^e = 0.797$  and  $C_E^e = 39.44$  at.% and for a range of plausible diffusive speeds in the range  $0.5$ - $5.0$  m s<sup>-1</sup> (for comparison [30] adopted  $V_D = 1.0$  m s<sup>-1</sup>), reveals that at elevated growth velocity the eutectic point moves systematically to higher Cu concentrations, with a significant shift in the eutectic concentration being observed for growth velocities of more than a few % of  $V_D$ , as shown in Figure 9. Although the measured *average* growth velocity for Ag-Cu eutectics is low, typically <  $0.003$  m s<sup>-1</sup> at all undercoolings for which eutectic growth is observed [5], instantaneous velocities may be much higher. Clopet *et al.* [26] observed ‘spasmodic’ growth in Ag-Cu, by which they meant that the recalescence front advanced by a series of jumps, separated by periods in which the front was stationary. During the early stages of recalescence, when the anomalous eutectic is predominant, these jumps covered a significant fraction of the visible area of the undercooled droplets and were not resolved by their high speed filming. At  $\Delta T = 40$  K, filmed at 250 frames per second, the largest jump covered 19% of the length of the droplet whereas at  $\Delta T = 51$  K, filmed at 500 frames per second, the largest jump covered 9% of the length of the droplet. For a 5 mm droplet, the minimum jump velocity in order to be unresolved during filming would therefore be around  $0.23$  m s<sup>-1</sup> in both cases. According to Figure 9 this would shift the local kinetic eutectic concentration by  $8.5 - 15$  at.% towards the Cu-rich end of the phase diagram, depending upon the value of  $V_D$  is adopted. The implication is that during the periods of rapid growth an alloy at the equilibrium eutectic composition would behave as if it were a hypoeutectic (Ag-rich) alloy with respect to the kinetic eutectic point. From [33] we note that if  $V > V_D$  a non-eutectic structure is observed due to diffusionless solidification. No such structures were observed here so we deduce that for no undercooling did the maximum local  $V$  exceed  $V_D$ .

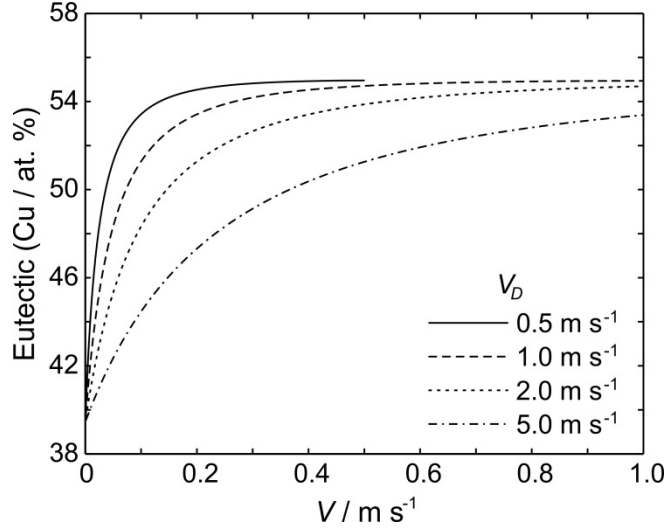


**Figure 9.** Kinetic shift in the eutectic point according to the model of [30] as a function of growth velocity,  $V$ , and characteristic diffusive speed in the melt,  $V_D$ .

As with analytical models of equilibrium eutectic growth [27], the solute field,  $C_L$ , ahead of the growing eutectic front in these non-equilibrium models [29, 30], is described by a Fourier series:

$$C_L(X, Z) = C_\infty + \sum_{n=0}^{\infty} B_n \cos(b_n X) \exp\left(-\frac{V}{D_L \psi} \omega_n Z\right) \quad (8)$$

$$\omega_n = \frac{1}{2} \left[ 1 + \sqrt{1 + \psi \left(\frac{2n\pi}{P_e}\right)^2} \right] \quad (9)$$

Here  $X$  is the co-ordinate parallel to the eutectic growth front and  $Z$  the co-ordinate in the growth direction which is co-moving at velocity  $V$  with the eutectic front,  $D_L$  is the diffusivity in the liquid,  $C_\infty$  the far-field concentration of the liquid,  $b_n = 2n\pi/\lambda$ ,  $P_e = V\lambda/2D_L$  and  $B_n$  are the Fourier coefficients, expressions for which are given in [30].

Figure 10a shows an example solution to Equ. (8) for  $C_L(X, Z)$ . The behaviour of the solution is explored in more detail in Figure 10b, where we show the value of  $C_L$  averaged in the  $X$  direction as a function of  $Z$  for various value of  $V_D$ . The behaviour of the solution is analogous to that of the solution for the near-equilibrium system with an off-eutectic composition in that there is, on average, a long range diffusion field in the growth direction ahead of the eutectic front, in addition to the normal transverse diffusion field. The consequence of this is that, because the kinetic eutectic point has moved to a more Cu-rich composition, a solute rich boundary layer will form ahead of the eutectic front, with the average concentration at the interface approaching that of the local (kinetic) eutectic composition. Despite the melt being Ag-rich with respect to the kinetic eutectic point, the solute boundary layer is Cu-rich, meaning that the residual liquid becomes enriched in Cu.

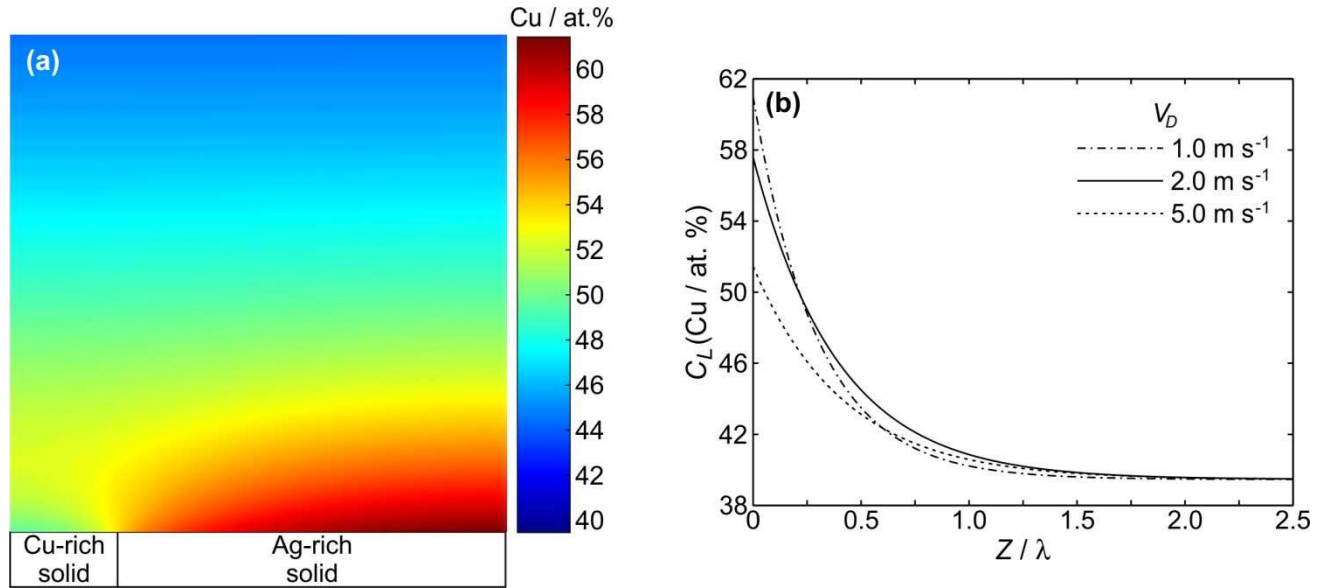


**Figure 10.** (a) 2D diffusion field calculated using the model of [30] for solidification of a eutectic growing at  $V = 0.23 \text{ m s}^{-1}$  with a diffusive speed in the liquid of  $V_D = 2.0 \text{ m s}^{-1}$ . Far field concentration of the liquid is that of the equilibrium eutectic. (b), average concentration in a linear segment parallel to the eutectic front showing a long-range diffusion field along the growth.

We therefore propose that during the rapid solidification phase of growth the solidification morphology is that of the normal lamellar eutectic, but growing with respect to a kinetic eutectic point shifted towards the Cu-rich end of the phase diagram. This is likely to be in the form of eutectic cells or dendrites, which are stabilised not only by the negative temperature gradient provided by the undercooled parent melt, but also by the solute rich boundary layer resulting from effectively off-eutectic growth (i.e. the melt, at the equilibrium eutectic composition, is off-eutectic with respect to the kinetic eutectic point). At the end of the recalescence phase of solidification the residual liquid will be enriched in Cu with respect to the equilibrium eutectic. Now, it is clear from Figure 1 that the extent of the coupled zone decreases with decreasing undercooling, becoming singular at the eutectic temperature. Therefore, given an undercooling in the residual liquid following recalescence of maybe 1-2 K, it would require only a very marginal enrichment of the residual liquid in Cu to take it outside of the coupled zone, wherein uncoupled growth would result in the solidification of Cu-rich dendrites, leaving a residual Ag-rich liquid. The formation of numerous small dendrites would be consistent with the second, diffuse recalescence event observed by [5] in Ag-Cu eutectics.

Assuming copious nucleation of these Cu-rich dendrites, which is not unreasonable given the presence of both solid Cu- and Ag in the eutectic phase, the as-solidified structure in the spaces between the eutectic cells/dendrites would consist of numerous small isolated Cu-rich dendritic fragments in a continuous Ag-rich matrix. Such a structure would strongly resemble the anomalous eutectic observed here and does, we believe, offer a plausible origin of the anomalous eutectic *without* invoking extensive remelting of the primary solid (Ag-Cu eutectic cells/dendrites). As such, the model proposed here aligns with that of [3, 7, 11, 14, 21] who have previously suggested a role

for uncoupled growth in the formation of the anomalous eutectic, although the mechanism giving rise to this uncoupled growth is different.

A number of predictions follow from this model which in principle allows it to be distinguished from typical remelting models such as those of [12, 18, 19]. The first is that the distribution of anomalous material will be different. If we consider the model for the remelting of eutectic dendrites proposed by [19], as summarised in their Figure 5a, cells of anomalous material are expected to be surrounded by lamellar eutectic at the cell margins. In contrast, we predict the opposite, with cells of lamellar eutectic surrounded by anomalous eutectic at the margins, the anomalous eutectic growing post-recalescence. The second is that we would predict, in the case of Ag-Cu eutectic, that the anomalous material would contain a higher proportion of Cu-rich material than would be expected. Both may be tested and are discussed in turn below.

Figure 11 shows two example microstructures obtained from samples undercooled by (a)  $\Delta T = 27$  K and (b)  $\Delta T = 40$  K. In both cases there is a clear cellular structure comprising the regular lamellar eutectic fringed with anomalous eutectic at the cell margins. Indeed, in Figure 11a there is even evidence of branching in the cellular envelope of the regular eutectic, which is strongly suggestive that this was the primary solidification morphology. There is no evidence of remelting in the cell centre, as would be suggested by the model of [19], with the centre remaining fully lamellar.

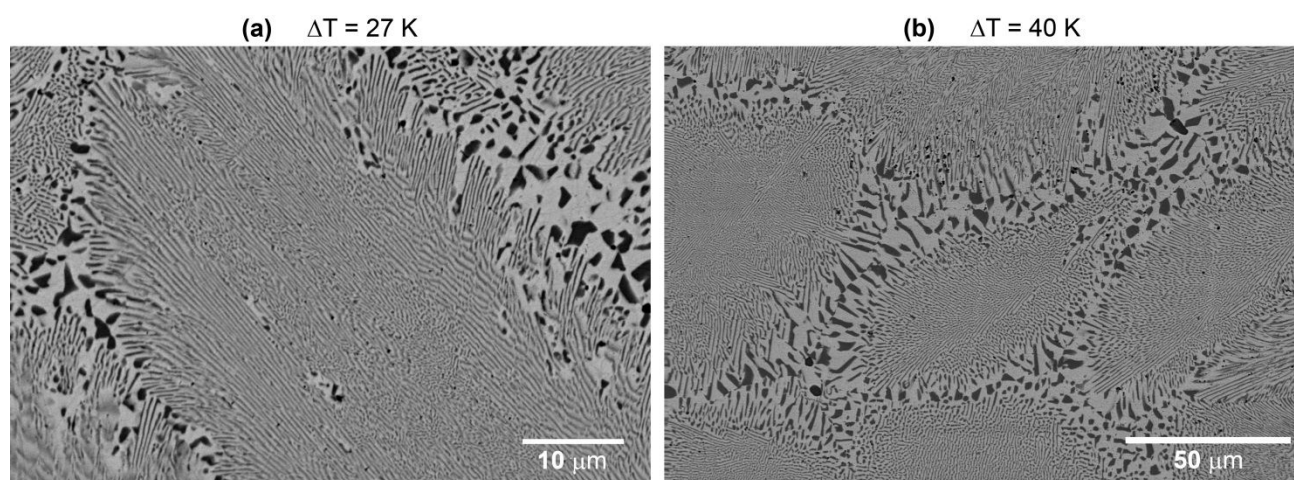


**Figure 11.** Two example microstructures from samples undercooled by (a) 27 K and (b) 40 K showing clear cells of lamellar eutectic fringed by anomalous eutectic at their margins.

In this regard it is interesting to compare our Figure 11 with Figure 6 in [19], both of which show anomalous eutectic formation in Ag-Cu alloy at the eutectic composition. In both cases the appearance of the anomalous eutectic is similar, comprising a random distribution of Cu-rich particles in a continuous Ag-rich matrix. Moreover, the characteristic length scale of the Cu-rich particles is, in both cases, similar being typically 2 – 3  $\mu\text{m}$ , although in our samples the anomalous eutectic appears to be located at the cell margins with lamellar cell centres. In the sample shown by [19] this is reversed, with the anomalous material in the cell centres and lamellar eutectic at the cell

margins. However, there is also a very significant difference in the size of the lamellar eutectic between the two samples. The typical lamellar spacing in Figure 11a is  $0.83\ \mu\text{m}$ , whereas in the sample shown in [19] it is around  $6\ \mu\text{m}$ , i.e. in the samples reported here the anomalous eutectic is very much coarser than the lamellar material, while in [19] it is significantly finer than the lamellar material. [19] does not comment upon this feature of the micrograph, but as remelting would normally be expected to also involve a degree of coarsening, this aspect of Figure 6 in [19] is not fully consistent with a pure remelting origin for the anomalous eutectic. However, perhaps the more interesting question is why there should be such an extreme difference between two microstructures obtained from nominally the same material and by similar techniques (melt fluxing). The primary difference in experimental method as far as we can determine is that [19] use direct induction heating of the sample in their experiment, whereas we use indirect heating via a graphite susceptor. Consequently, in our system heating is, in effect, via a blackbody radiation furnace. The large (relative to the sample) thermal mass of the susceptor means that the cooling rate in our experiment should be much slower than in [19], although as this would be expected to lead to a coarser, rather than a finer, structure we do not feel this is significant. Perhaps a more significant difference is that direct induction heating of the sample will induce stirring within the sample. In levitated samples this has been shown to very significantly affect the results obtained in undercooling experiments [34]. We therefore conjecture that the anomalous eutectic observed in [19] may, at least in part, be due to stirring induced fragmentation. As heating in our undercooling experiments was via thermal radiation, such stirring would have been absent, accounting for the difference between the results obtained here and those in [19].

We now return to the extreme difference in scale between the lamellar and anomalous eutectic in our experiments. It is well established that although the growth of eutectics is cooperative, their melting is non-cooperative [35], so that during partial remelting, *if it were the origin of the anomalous eutectic*, we would expect the Cu-rich lamellar to remain solid while some or all of the Ag-rich lamellar melted. In order to transform these Cu-rich lamellar into the anomalous structure some break-up of the lamellar, presumably via some form of Rayleigh type instability is required. This is true irrespective of whether the anomalous eutectic is truly globular (in which case the instability must fragment the sheet-like lamellar along both of its long dimensions) or is interconnected in 1-dimension, as has been shown to be the case with Ni-Sn [10] (in which case the instability must fragment the lamellar along only 1 of its 2 long dimensions). Either way, the resulting structure will have a characteristic size in its short dimension(s) which is of the order of the lamellar thickness. Taking the structure in Figure 11a as an example, the measured mean lamellar spacing in this structure is  $0.83\ \mu\text{m}$ , giving the width of the Cu-rich lamellar as  $0.26\ \mu\text{m}$  (for equilibrium solidification, or  $0.18\ \mu\text{m}$  based upon the model of [30] with  $V_D = 2\ \text{m s}^{-1}$ ). In contrast, Cu-rich particles within the anomalous eutectic have diameters up to  $3\ \mu\text{m}$ , wherein extensive coarsening would also need to be postulated to give the observed structure. Indeed, the case shown in Figure 11a is not the most extreme example of this we have observed. In the sample undercooled by

$\Delta T = 40$  K Cu-rich particles up to  $3.8 \mu\text{m}$  in diameter are found within the anomalous eutectic and are observed to co-exist with lamellar eutectic having a mean spacing of  $0.31 \mu\text{m}$ , wherein the Cu-rich lamellar will have an expected width of  $0.1 \mu\text{m}$  (for equilibrium solidification, or  $0.07 \mu\text{m}$  for  $V_D = 2 \text{ m s}^{-1}$ ). This scale difference alone we consider to be strong evidence against remelting models for the origin of the anomalous eutectic structures observed here.

We now turn to the composition of the anomalous eutectic. As discussed in Section 3 above, the composition of the individual Ag- and Cu-rich regions has been measured by EDX and been found to be close to the equilibrium values, indicating the anomalous eutectic grew at low undercooling. This would be consistent with either the model proposed above or any of the current remelting models. However, the model proposed above suggests that the anomalous eutectic should be Cu-rich, although this will be reflected in the overall proportion of the Cu-rich phase present in the anomalous eutectic, rather than by the composition of the individual regions. With reference to Figure 3 it can be seen that the image analysis techniques applied here can not only be used to quantify the volume fraction of anomalous eutectic, but also the proportions of the Ag- and Cu-rich phases comprising the anomalous eutectic. For each undercooled sample this ratio has been determined at every sampling point within the specimen. By assuming the Ag- and Cu-rich phases have their equilibrium composition this has then been converted to give the Cu concentration at each sampling point. We have then calculated the average Cu concentration of the anomalous eutectic, weighted by the fraction of anomalous material at the sampling point. This is shown, as a function of undercooling, in Figure 12. For low values of  $\Delta T$  the Cu concentration of the anomalous eutectic increases with increasing undercooling ( $< 30$  K). Thereafter, the concentration is approximately independent of undercooling, with all measured value being above the equilibrium value, as predicted by the model.

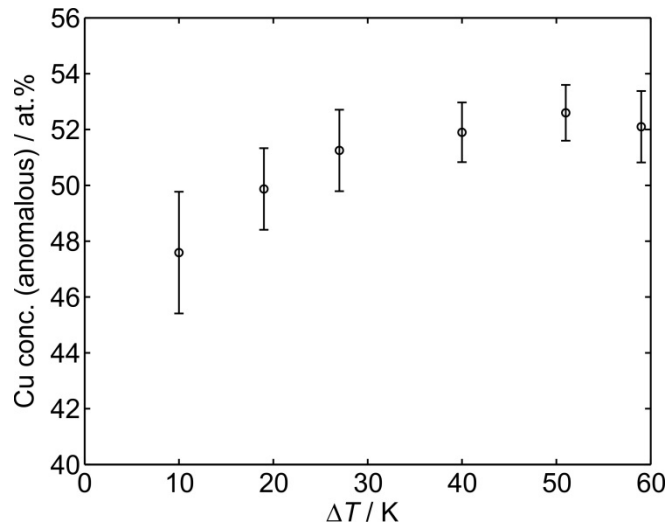


**Figure 12.** Estimated average Cu concentration of the anomalous eutectic, estimated from the fraction of Cu-rich material, plotted as a function of sample undercooling.

Finally, we turn to what role, if any, remelting does play in the formation of the anomalous eutectic. There is an extensive literature on the role of remelting during rapid solidification

processing, particularly in relation to the spontaneous grain refinement effect. The proposed effect of remelting is invariably a reduction in length scale [see e.g. 36]. However, here the opposite is the case, the anomalous eutectic is at least an order of magnitude coarser than the lamellar structure. Consequently, we do not believe remelting of the lamellar structure can *directly* produce the anomalous structure. We conjecture that remelting does occur, probably to a limited extent, and that it produces Cu-rich particles with a size comparable to the Cu lamellar thickness. These fine Cu particles act as nucleating seeds for the Cu-rich phase within the anomalous eutectic, which would explain why there are numerous small globular particles, rather than extended dendrites.

## 5. Summary and Conclusions

By using quantitative image analysis the spatial distribution of anomalous eutectic has been mapped within Ag-Cu samples undercooled in the range 10 – 60 K using a melt fluxing technique. The distribution is found to be extremely heterogeneous, with the majority of the anomalous material being observed close to the nucleation site. By measurement of lamellar spacing this decrease in anomalous material away from the nucleation site can be attributed to a decrease in droplet undercooling as solidification proceeds. However, the most significant finding is the large volume fraction of anomalous material that can be generated at very modest undercoolings. For many of the samples this exceeds the estimated recalescence solid fraction by around an order of magnitude. As such, these results are completely incompatible with current models for anomalous eutectic formation, which ascribe this morphology to the partial remelting of a regular eutectic, usually in the form of cells or dendrites. An alternative model, based on a kinetic shift in the eutectic point during rapid solidification, is proposed. The distribution and solute content of the anomalous eutectic is shown to be in good agreement with the predictions of this kinetic model.

## 6. References

- [1] G.L.F Powell and L.M. Hogan: Undercooling in silver-copper eutectic alloys. *J. Inst. Metals*, **93** (1965) 505–512.
- [2] S. Walder and P.L. Ryder: Nonequilibrium solidification in undercooled melts of the alloy Ag-39.9 at percent-Cu, *J. Appl. Phys.* **73** (1993) 1965–1970.
- [3] N. Wang, C. D. Cao and B. Wei: Solidification behaviour of silver-copper alloys in a drop tube. *Adv. Space Res.* **24** (1999) 1257–1261.
- [4] S. Zhao, J.F. Li, L. Liu and Y.H. Zhou: Cellular growth of lamellar eutectics in undercooled Ag-Cu alloy, *Mater. Charact.* **60** (2009) 519–524.
- [5] C.R. Clopet, R.F. Cochrane and A.M. Mullis: The origin of anomalous eutectic structures in undercooled Ag-Cu alloy, *Acta Mater.* **61** (2013) 6894–6902.
- [6] E. Cadirli, D.M. Herlach and T. Volkman: Characterization of rapidly solidified Ni-Si and Co-Al eutectic alloys in drop tube. *J. Non-cryst. Sol.*, **356** (2010) 461–466.
- [7] B. Wei, D.M. Herlach, F. Sommer and W. Kurz: Rapid dendritic and eutectic solidification of

- undercooled Co-Mo alloys, *Mater. Sci. Eng. A* **181-182** (1994) 1150–1155.
- [8] R. Goetzinger, M. Barth and D.M. Herlach: Mechanism of formation of the anomalous eutectic in rapidly solidified Ni-Si, Co-Sb and Ni-Al-Ti alloys. *Acta Mater.*, **46** (1998) 1647–1655.
- [9] L. Liu, J.F. Li and Y.H. Zhou: Solidification interface morphology pattern in the undercooled Co-24.0 at.% Sn eutectic melt. *Acta Mater.*, **59** (2011) 5558–5567.
- [10] T.Z. Kattamis and M.C. Flemings: Structure of undercooled Ni-Sn eutectic. *Metall. Trans.*, **1** (1970) 1449–1451.
- [11] M. Li, K. Nagashio and K. Kuribayashi: Re-examination of the solidification behavior of undercooled Ni–Sn eutectic melts, *Acta Mater.* **50** (2002) 3239–3250.
- [12] J.F. Li, W.Q. Jie, S. Zhao and Y.H. Zhou: Structural evidence for the transition from coupled to decoupled growth in the solidification of undercooled Ni-Sn eutectic melt. *Metall. Mater. Trans. A*, **38A** (2007) 1806–1816.
- [13] B. Wei, D.M. Herlach, F. Sommer and W. Kurz: Rapid solidification of undercooled eutectic and monotectic alloys. *Mater. Sci. Eng. A* **173** (1993) 355–359.
- [14] B.L. Jones: Growth mechanisms in undercooled eutectics. *Metall. Trans.*, **2** (1971) 2950–2951.
- [15] J.F. Li, X.L. Li, L. Liu and S.Y. Lu: Mechanism of anomalous eutectic formation in the solidification of undercooled Ni–Sn eutectic alloy. *J. Mater. Res.*, **23** (2008) 2139–2148.
- [16] S.N. Tewari: Effect of undercooling on the microstructure of Ni-35 at. pct Mo (eutectic) and Ni-38 at. pct Mo (hypereutectic) alloys. *Metall. Trans. A.*, **18A** (1987) 525–542.
- [17] S. Zhao, J.F. Li, L. Liu and Y.H. Zhou: Eutectic growth from cellular to dendritic form in the undercooled Ag-Cu eutectic alloy melt. *J. Cryst. Growth.*, **311** (2009) 1387–1391.
- [18] C. Yang, J. Gao, Y.K. Zhang, M. Kolbe and D.M. Herlach. New evidence for the dual origin of anomalous eutectic structures in undercooled Ni–Sn alloys: In situ observations and EBSD characterization. *Acta Mater.*, **59** (2011) 3915–3926.
- [19] X.X. Wei, X. Lin, W. Xu, Q.S. Huang, M. Ferry, J. F. Li and Y. H. Zhou: Remelting-induced anomalous eutectic formation during solidification of deeply undercooled eutectic alloy melts. *Acta Mater.* **95** (2015) 44–56.
- [20] J.F. Li and Y.H. Zhou: Eutectic growth in bulk undercooled melts. *Acta Mater.*, **53** (2005) 2351–2359.
- [21] C. Lai, H. Wang, Q. Pu, T. Xu, J. Wang, X. Zhang & F. Liu: Phase selection and re-melting-induced anomalous eutectics in undercooled Ni–38 wt% Si alloys. *J Mater. Sci.* **51** (2016) 10990–11001.
- [22] J.L. Murray: Calculations of stable and metastable equilibrium diagrams of the Ag-Cu and Cd-Zn Systems. *Metall. Trans. A*, **15A** (1984) 261–268.
- [23] R. Elliott: Eutectic Solidification Processing: Crystalline and Glassy Alloys. Butterworths, London (1983). ISBN: 978-1483112398.
- [24] E.G. Castle, A.M. Mullis and R.F. Cochrane: Mechanism selection for spontaneous grain refinement in undercooled metallic melts, *Acta Mater.* **77** (2014) 76-84

- [25] K. Dragnevski, A.M. Mullis and R.F. Cochrane: The effect of experimental variables on the levels of melt undercooling. *Mater. Sci. Eng. A*, **375-377** (2004) 485–487.
- [26] C.R. Clopet, R.F. Cochrane and A.M. Mullis: Spasmodic growth during the rapid solidification of undercooled Ag-Cu eutectic melts, *Appl. Phys. Lett.* **102** (2013) 031906.
- [27] K.A. Jackson and J.D. Hunt: Lamellar and rod eutectic growth, *Trans. Metall. Soc. AIME* **236** (1966) 1129–1142.
- [28] F.H. Hayes, H.L. Lukas, G. Effenberg, and G. Petzow: A thermodynamic optimisation of the Cu-Ag-Pb system, *Z. Metallkde* **77** (1986) 749–754.
- [29] H. Wang, F. Liu and D.M. Herlach: On the solution of solute diffusion during eutectic growth, *J. Cryst. Growth* **389** (2014) 68–73.
- [30] W. Kuang, H. Wang, F. Liu, S.L. Sobolev: Modeling of eutectic dendrite growth in undercooled binary alloys, *J. Mater. Sci.* **51** (2016) 2141–2152.
- [31] P. K. Galenko: Extended thermodynamical analysis of a motion of the solid-liquid interface in a rapidly solidifying alloy, *Phys. Rev. B* **65** (2002) 144103.
- [32] P. K. Galenko: Solute trapping and diffusionless solidification in a binary system, *Phys. Rev. E*. **76** (2007) 031606.
- [33] P.K. Galenko, D.M. Herlach: Diffusionless crystal growth in rapidly solidifying eutectic systems, *Phys. Rev. Lett.* **96** (2006) 150602.
- [34] S. Binder, P.K. Galenko, D.M. Herlach: The effect of fluid flow on the solidification of Ni<sub>2</sub>B from the undercooled melt, *J. Appl. Phys.* **115** (2014) 053511.
- [35] A. Clarke, D. Turret, S. Imhoff, P. Gibbs, K. Fezzaa, J. Cooley, W-K. Lee, A. Deriy, B. Patterson, P. Papin, K. Clarke, R. Field, J. Smith: X-ray Imaging and Controlled Solidification of Al-Cu Alloys Toward Microstructures by Design, *Adv. Eng. Mater.* **17** (2015) 454-459.
- [36] M. Schwarz, K. Karma, K. Eckler, D. M. Herlach: Physical-mechanism of grain-refinement in solidification of undercooled melts, *Phys. Rev. Lett.* **73** (1994) 1380-.